Integrated Design of Space Structures Using Lattice Plate Finite Elements

S. E. Lamberson*
U.S. Air Force Academy, Colorado Springs, Colorado
and
T. Y. Yang†
Purdue University, West Lafayette, Indiana

Lattice plate finite elements based on a continuum model of a large plate-like lattice space structure are used to examine the effect of variation of several fundamental structural parameters on the natural frequencies and mode shapes of the structure. Reduced-order controller design models are developed using modal cost analysis to rank the modes for each set of structural parameter values. The linear-quadratic-Gaussian controller design method is used to develop feedback control systems for each set of structural parameter values. The resulting system performance is then evaluated by examining the steady-state regulation cost of the structure as a function of the structural design parameters.

Introduction

As the size and flexibility of large space structures increase, feedback control systems often become necessary not only to control the rigid-body motion of the space platform, but also to suppress undesirable mechanical vibrations. These structures often are composed of a large number of repetitions of a basic pattern or unit cell, each containing a number of truss-type members. A variety of continuum modeling methods have been developed which allow the natural frequencies and mode shapes of a lattice space structure to be calculated.[1-3] Instead of modeling each individual structural member of the lattice space structure using conventional matrix methods, these continuum modeling methods use a set of partial differential equations to describe an "equivalent" continuum having the same planform as the lattice space structure. One of these methods has been extended[4,5] by developing an equivalent beam or plate-like finite element from the partial differential equations. The finite element based on the equivalent continuum formulation allows more flexibility in treating geometry, boundary conditions, attachments, and other structural complexities when calculating the natural frequencies and mode shapes than do other solution methods. These equivalent finite elements have been demonstrated[4,5] as effective tools for feedback control system design of lattice space structures. Using an equivalent plate-like finite element,[5] this paper conducts a parametric study of the effect of basic lattice configurations on the natural frequencies, mode shapes, and the resulting control system performance, while the total mass of structure is held constant.

Theoretical Background

Equivalent Plate Models

The method developed in Ref. 3 is used to generate strain-energy and kinetic-energy expressions for the structure in terms of strain components of the plate at the midplane. Briefly, the displacements are assumed to vary linearly through the thickness of the plate.

$$u(x,y,z) = u^0(x,y) + \phi_x(x,y)$$

$$v(x,y,z) = v^0(x,y) + \phi_y(x,y)$$

$$w(x,y,z) = w^0(x,y) + \phi_3^0(x,y) \tag{1}$$

where

(x,y,z) = coordinates of a point within the plate-like lattice
(u,v,w) = displacements along (x,y,z)
(ϕ_x,ϕ_y) = rotations about the $(-y,x)$ axes at the midplane $(z=0)$
(u^0,v^0,w^0) = displacements along (x,y,z) at the midplane
$\phi_3^0 = dw/dz$ at the midplane

The axial strain in the truss members of a typical unit cell is expressed in terms of strain components.

$$k = \sum_{i=1}^{3}\sum_{i=1}^{3} \epsilon_{ij}^k l_i^k l_j^k \tag{2}$$

where

ϵ^k = axial strain in the kth truss bar
ϵ_{ij}^k = strain components of ϵ^k
l_i^k = direction cosines of the member

These are then expanded using a Taylor series in terms of the strain components and their derivatives about some arbitrary origin within the unit cell. The fact that the forces associated with certain of the strain components and derivatives are zeros is used to reduce the strain-energy expression to an expression in terms of eight strain components at the plate midplane. The truss cell geometry used in this study is analyzed in Ref. 3.

$$U_{\text{cell}} = \frac{1}{2}\{\epsilon_l^0\}^T [W_{\text{eq}}] \{\epsilon_l^0\} \tag{3}$$

where

U_{Cell} = strain energy of a unit cell
$[W_{\text{eq}}]$ = equivalent constitutive matrix
$\{\epsilon_l^0\} = [\epsilon_{11}^0, \epsilon_{22}^0, \epsilon_{12}^0, \kappa_{11}^0, \kappa_{22}^0, \kappa_{12}^0, \epsilon_{13}^0, \epsilon_{23}^0]^T$

and ϵ_{ij}^0, κ_{ij}^0, and ϵ_{i3}^0 are defined as in Eq. (4) with $x=y=0$.

Presented as Paper 85-0592 at the AIAA/ASME/ASCE/AHS 26th Structures, Structural Dynamics and Materials Conference, Orlando, FL, April 15-17, 1985; received June 17, 1985; revision received Jan. 8, 1986.

*Assistant Professor of Engineering Mechanics. Member AIAA.
†Professor of Aeronautics and Astronautics, Dean of Engineering. Fellow AIAA.

In order to develop a transverse shear-type plate finite element based on the equivalent continuum model it is assumed that this strain-energy expression is valid at all points within the structure regardless of their location within the lattice.

$$\frac{d^2U}{dx_1dx_2} = \frac{1}{2}\{\epsilon_l(x,y)\}\frac{T[W_{eq}]}{A_{cell}}\{\epsilon_l(x,y)\} \tag{4}$$

where

U = strain energy of the plate-like structure
A_{cell} = area of the lattice unit cell
$\{\epsilon_l(x,y)\} = [\epsilon_{11},\epsilon_{22},\epsilon_{12},\kappa_{11},\kappa_{22},\kappa_{12},\epsilon_{13},\epsilon_{23}]^T$

$$\epsilon_{11}=\frac{du}{dx},\quad \epsilon_{22}=\frac{dv}{dy},\quad \epsilon_{12}=\frac{1}{2}\left(\frac{dv}{dx}+\frac{du}{dy}\right)$$

$$\kappa_{11}=\frac{d\phi_x}{dx},\quad \kappa_{22}=\frac{d\phi_y}{dy},\quad \kappa_{12}=\frac{1}{2}\left(\frac{d\phi_y}{dx}+\frac{d\phi_x}{dy}\right)$$

$$\epsilon_{13}=\frac{1}{2}\left(\frac{dw}{dx}+\phi x\right),\quad \epsilon_{23}=\frac{1}{2}\left(\frac{dw}{dy}+\phi y\right)$$

Since this is assumed valid for all points in the structure, the strain energy of an arbitrary plate finite element within the plate-like lattice structure is

$$U_{el}=\frac{1}{2}\int\int_{A_{el}}\{\epsilon_l\}\frac{T^{[W_{eq}]}}{A_{cell}}\{\epsilon_l\}dydx \tag{5}$$

where U_{el} is the strain of an equivalent plate finite element, and A_{el} the area of the element.

The 16 degree-of-freedom (d.o.f.) rectangular plate element[6] is modified to include transverse shear terms and in-plane terms yielding a 32-d.o.f. element (Fig. 1). The interpolation functions are assumed to be bilinear except for the out-of-plane displacement, which is assumed as a bicubic Hermite polynomial.

$$u=a_1+a_2x+a_3y+a_4xy$$

$$v=a_5+a_6x+a_7y+a_8xy$$

$$w=a_9+a_{10}x+a_{11}y+a_{12}x^2+a_{13}xy+a_{14}y^2+a_{15}x^3$$
$$+a_{16}x^2y+a_{17}xy^2+a_{18}y^3+a_{19}x^3y+a_{20}x^2y^2$$
$$+a_{21}xy^3+a_{22}x^3y^2+a_{23}x^2y^3+a_{24}x^3y^3$$

$$\epsilon_{23}=a_{25}+a_{26}x+a_{27}y+a_{28}xy$$

$$\epsilon_{23}=a_{29}+a_{30}x+a_{31}y+a_{32}xy \tag{6}$$

The displacement functions in Eq. (6) are used along with the strain definition in Eq. (4) to relate the strain vector $\{\epsilon_l\}$ to the vector of displacement coefficients $\{a\}$.

$$\{\epsilon_l\}=[B]\{a\} \tag{7}$$

where

$$\{a\}=[a_1,a_2,\ldots,a_{32}]^T$$

Substituting Eq. (7) into Eq. (5) gives the strain-energy expression of the plate finite element in terms of the displacement function coefficients.

$$U_{el}=\frac{1}{2}A_{cell}\int\int_{A_{el}}\{a\}^T[B]^T[W_{eq}][B]\{a\}dydx \tag{8}$$

By substituting the x and y coordinates of each of the plate d.o.f. on the right-hand side of Eq. (6), an expression relating each of the element d.o.f. to the displacement function coefficients $\{a\}$ is obtained. For example,

$$u_3=a_1+aa_2+ba_3+aba_4 \tag{9}$$

where

u_3 = displacement in the x direction at node 3 of the element
a,b = width of element in x and y directions, respectively

This results in a set of 32 simultaneous equations in 32 unknowns.

$$\{g\}=[s]\{a\} \tag{10}$$

where

$$\{g\}=[\{g_1\}^T,\{g_2\}^T,\{g_3\}^T,\{g_4\}^T]$$

$\{g_i\} = [u_i,v_i,w_i,\frac{dw_i}{dx},\frac{dw_i}{dy},\frac{d^2w_i}{dxdy},\epsilon_{13i},\epsilon_{23i}]^T$, the element d.o.f. at the ith node point of the finite element

This set of equations can be solved to relate the displacement coefficients $\{a\}$ to the element d.o.f. $\{g\}$.

$$\{a\}=[T]\{g\} \tag{11}$$

Substituting Eq. (11) into Eq. (8) gives the strain-energy expression of the element in terms of the element d.o.f. $\{g\}$.

$$U_{el}=\frac{1}{2A_{cell}}\{g\}^T\int\int_{a_{el}}[T]^T[B]^T[W_{eq}][B][T]dydx\{g\} \tag{12}$$

According to Castigliano's theorem the strain energy of the element is related to the stiffness matrix of the element.

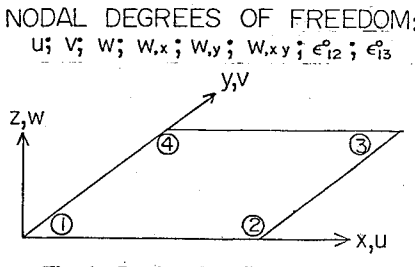

Fig. 1 Lattice plate finite element.

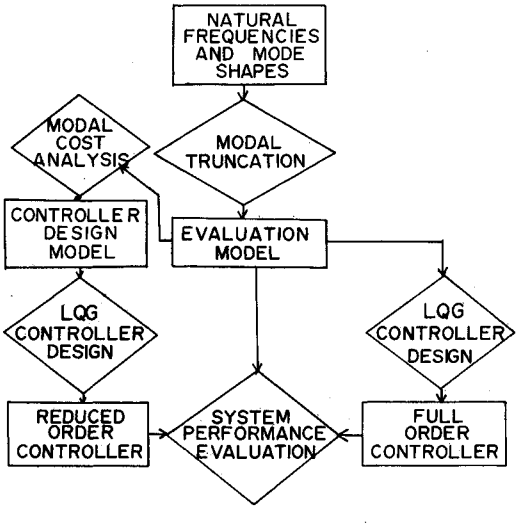

Fig. 2 Control system design procedure.

$$U_{el}=\frac{1}{2}\{g\}^T[K_{el}]\{g\}\mathrm{d}y\mathrm{d}x \tag{13}$$

where $[k_{el}]$ is the element stiffness matrix.

Comparing Eqs. (13) and (12), it follows that

$$[K_{el}]=\frac{1}{a_{\text{cell}}}\int\int_{A_{el}}[T]^T[B]^T[W_{\text{eq}}][B][T]\mathrm{d}y\mathrm{d}x \tag{14}$$

The kinetic-energy expression derived in Ref. 3 is used to generate a lumped mass matrix including both mass and rotatory inertia terms as described in Ref. 5.

$$T_{el}=\frac{1}{2}\{\dot{g}\}^T[M_{el}]\{\dot{g}\} \tag{15}$$

where T_{el} is the kinetic energy of the element, and $[M_{el}]$ the element lumped mass matrix. Once the stiffness and mass matrices for each element are available, they are assembled to yield stiffness and mass matrices for the equivalent plate finite element model of the plate-like lattices.

$$U=\frac{1}{2}\{g\}^T[K]\{g\}=\sum_{\text{All elements}}U_{el} \tag{16}$$

where

$\{g\}$ = d.o.f. of the equivalent plate finite element model of the plate-like lattice

$[K]$ = stiffness matrix of the entire model

$$T=\frac{1}{2}\{\dot{g}\}^T[M]\{\dot{g}\}=\sum_{\text{All elements}} \tag{17}$$

where T is the kinetic energy of the plate-like lattice structure, and $[M]$ the mass matrix of the entire model.

The free-vibration equations of motion of the plate-like lattice structure are given by Lagrange's equation.

$$\frac{\mathrm{d}}{\mathrm{d}t}\left(\frac{\partial T}{\partial \dot{g}_i}\right)+\frac{\partial U}{\partial g_i}=0 \tag{18}$$

Substituting Eqs. (16) and (17) into Eq. (18), the equation of motion is obtained for the finite element model of the structure.

$$[M]\{\ddot{g}\}+[K]\{g\}=0 \tag{19}$$

Making the standard assumption that g is harmonic yields the finite element eigenvalue, eigenvector problem.

$$[[K]-\omega^2[M]]\{Q\}=0 \tag{20}$$

where

$\{g\}=\{Q\}\sin\omega t$

$\{Q\}$ = normal mode associated with natural frequency ω

t = time

Solving Eq. (20) gives a set of natural frequencies and mode shapes of the same order as the stiffness and mass matrices.

Feedback Control System Design

Once the structural vibration characteristics have been calculated, several reduced-order linear-quadratic-Gaussian (LQG) controllers of different orders are designed using the method described in Ref. 5. (see Fig. 2). The modal model developed using the equivalent finite element model is reduced to an evaluation model, which is used as the system or plant model for control system design and closed-loop system performance evaluation. The evaluation model is obtained by retaining the lower frequency modes of the finite element solution which are controllable and observable. The high-frequency modes are eliminated both for convenience and because they are inherently less accurate than the low-frequency modes. This evaluation model, which is assumed to represent the dynamics of the finite order structure, must be of higher order than the order of the desired feedback control system so that spillover effects can be estimated. Therefore, some means of model reduction is necessary. Several dynamic reduction schemes have been developed to allow the control problem to influence the model reduction; of these, Modal Cost Analysis (MCA) is the most straight-forward to use.[7] The modal cost is calculated by determining the contribution to a specified quadratic cost function of each of the normal modes in the open-loop configuration.

The control design modal model or order n is derived from the evaluation model by retaining the $n/2$ modes having the largest modal costs. Since rigid-body modes have infinite modal cost, they must always be retained in the reduced models if they are controllable and observable. Each control system design model is used to calculate a standard LQG controller,[8] which is then used in the closed loop with the evaluation model of the structure to calculate the system performance in terms of the value of the quadratic cost function.

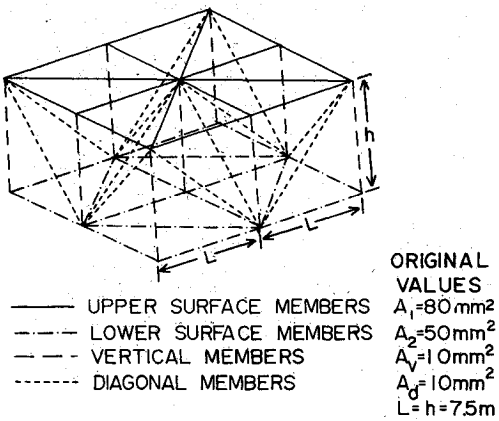

Fig. 3 Lattice space structure unit cell.

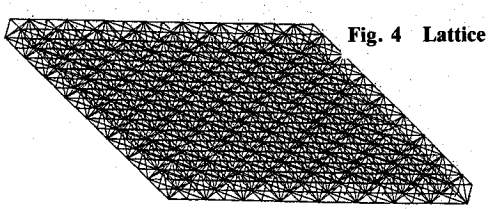

Fig. 4 Lattice space structure.

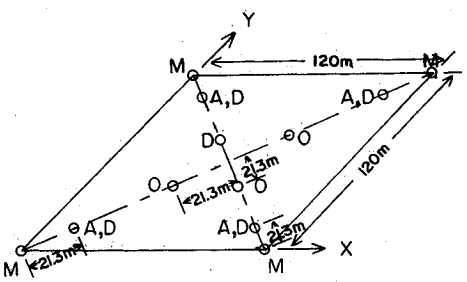

Fig. 5 Control system configuration.

Integrated Structure-Control System Design

In the past, spacecraft have often been designed by maximizing the natural frequencies of the structure, and then designing a feedback controller based on this given structure. An alternative is to design feedback controllers for a number of structural designs varying some of the fundamental properties of the structure and examining the effect of these changes on the performance of the closed-loop system. For large space structures this may not be practical due to the cost and/or time required to calculate the natural frequencies and mode shapes using detailed finite element models. However, the efficiency of equivalent continuum finite elements depends upon the number of modes desired, not the complexity of the actual structure. Therefore, once large space structures are modeled using equivalent continuum finite elements, such studies become practical. This is demonstrated in the following parametric study. It should be noted that for both parameters, which are varied, the structure that yields the optimum performance in the closed-loop system is different from the structure with the lowest natural frequencies. This demonstrates the need to consider the feedback control system when designing the structure.

Lattice Space Structure Configuration

The initial space lattice geometry used in this study was used previously to demonstrate the effectiveness of equivalent finite element models in designing feedback control systems for plate-like lattice space structures.[5] A simple unit cell (Fig. 3) is repeated eight times in two orthogonal directions to generate the lattice space structure (Fig. 4). The lattice space structure geometry is defined by six parameters. Four of these are the cross-sectional area of: the upper-surface members (A_1), the lower-structure members (A_2), the vertical members connecting the two surfaces (A_v), and the diagonal members connecting the two surfaces (A_d). The remaining two parameters are the thickness or height (h) and half-width (L) of the unit cell. For simplicity, it is assumed in this study that all members are of circular hollow cross sections with outer diameter (d_o) and inner diameter (d_i).The ratio between the two diameters (d_o/d_i) is defined as a. The plate-like lattice structure is assumed to be free along all four edges. The control system configuration, shown as a midplane in Fig. 5, consists of a set of four pairs of torque actuators (A) about the x and y axes, respectively, located along the diagonals of the plate-like structure a distance of 21.3 m from each corner. The eight actuators are driven by a feedback control system using eight sensors (M) measuring the angular motion of the structure. These angular sensors are located in pairs at the four corners of the structure. Five pairs of disturbances (D) are used: four pairs are at the same location as the actuators and one pair is 21.3 m from the center of the structure along a diagonal.

Cross-Sectional Area Variation

The first parametic variation performed in this study is optimizing the cross-sectional areas (A_1, A_2, A_v, and A_d) for fixed lengths (L and h). Examining the strain-energy terms calculated for the equivalent continuum formulation (see Table 2 of Ref. 3), it is apparent that the bending stiffnesses depend on the sum of A_1 and A_2. For simplicity of this study, the cross-sectional area (A_s) of all of the members in the upper and lower surfaces was assumed to be the same.

$$A_s = A_1 = A_2 \tag{21}$$

The cross-sectional area A_v was held constant at its original value. The total mass of the structure, which is held constant, is given by

$$M = \frac{2 \text{ area}}{L}\left[\left(1+\frac{1}{\sqrt{2}}\right)(A_1+A_2)+\frac{1}{2}\frac{h}{L}A_v+\frac{d}{L}A_d\right]m \tag{22}$$

where m is the density of the structural members, $d=\sqrt{h^2+L^2}$, and "area" is the area of the lattice plate structure. Substituting the assumed parameter values into Eq. (22) yields the following relation between A_s and A_d:

$$A_s = (69.167 - 4.167\times 10^5 A_d)\times 10^{-6}\text{m}^2 \tag{23}$$

The members of the lattice structure are extremely slender. Before examining the effect of varying A_s and A_d on the natural frequencies, mode shapes, and performance, their effect on the Euler buckling load capacity of each lattice member is examined and shown in Fig. 6. Since A_s is related to A_d by Eq. (23), only A_d is used in presenting the results. The buckling load of each tubular member is nondimensionalized by dividing its value by the buckling load of the initial lower-surface members

$$P_o = EI_o/L \tag{24}$$

where $E=71.7\times 10^6$ psi.

$$I_o = \frac{\pi(a^4-1)d_1^4}{b^4} \qquad d_o = ad_i$$

Figure 7 shows that as A_d is varied to either extreme, either A_d or the inversely related A_s will become very small, causing the members to have unacceptably low values of the Euler buckling load. For reference, the Euler buckling loads of the surface and diagonal members in the initial configuration are

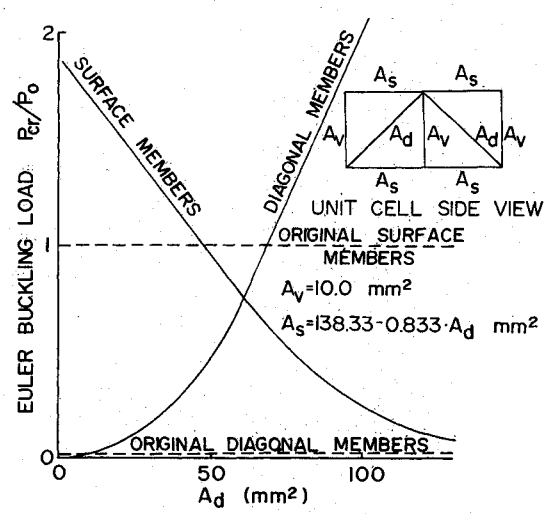

Fig. 6 Allowable buckling load vs diagonal member area.

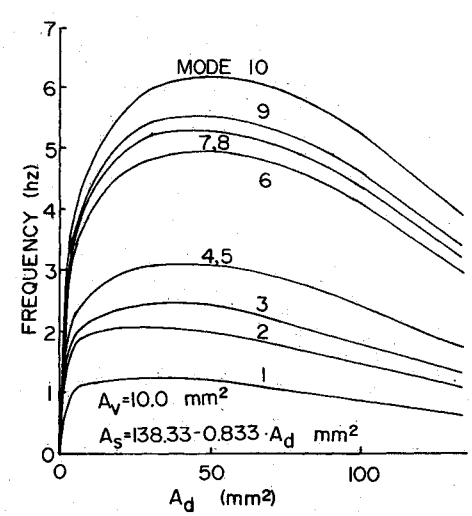

Fig. 7 Natural frequency vs diagonal member area.

shown in Fig. 6 as dashed lines. Figure 7 shows the effect of the cross-sectional area A_d (and the inversely related A_s) on the natural frequencies of various modes. It is noted that modes 4 and 5 and 7 and 8 are double modes. It is interesting to note that all of the present natural frequencies for the ten lowest modes approach maxima when A_d is between 30 and 50 mm^2. Apparently, the trends of these curves result from the compensating effects of three factors: the bending stiffness, the transverse shear stiffness, and the rotatory inertia. When A_d decreases (or A_s increases) both the bending stiffness and the rotatory inertia increase, whereas the transverse shear stiffness decreases. Figure 8 shows the effect of A_d on the open-loop modal cost of each mode. As the value of A_d decreases, the modal cost of the first mode becomes increasingly dominant, whereas the modal cost curves for several other modes cross each other. Such crossings indicate that different modes are retained at different A_d values in the reduced-order feedback control system design models.

For each set of parameter values, a series of reduced-order controllers is designed using the LQG method. The system performance is evaluated using the full evaluation model driven by the reduced-order controller. A typical performance curve (Fig. 9) relating regulation cost (V_y) to control energy (V_u) is generated by varying

$$V_{\text{total}} = V_y + \rho V_u \tag{25}$$

where

V_{total} = total quadratic cost
ρ = relative importance of control energy
V_y = cost associated with system output
V_u = energy regulation cost

The performance curves for all of the cases studied are very similar and are available in Ref. 9. Figure 10 shows V_y, the regulation cost, vs A_d for various constant values of ρ (+ marks) and for the minimum V_y (circled points.) These results are for a controller design retaining two rigid-body modes and three elastic modes in the reduced-order contoller design model. The results for other reduced-order controller orders were similar and also can be found in Ref. 9. The minimum regulation cost is obtained for A_d values between 10 and 30 mm^2. The structural design that yields the best closed-loop system performance occurs for diagonal brace areas which are half those that give maximum structural natural frequencies. This tends to demonstrate the requirement to consider closed-loop system design and performance when designing the structure.

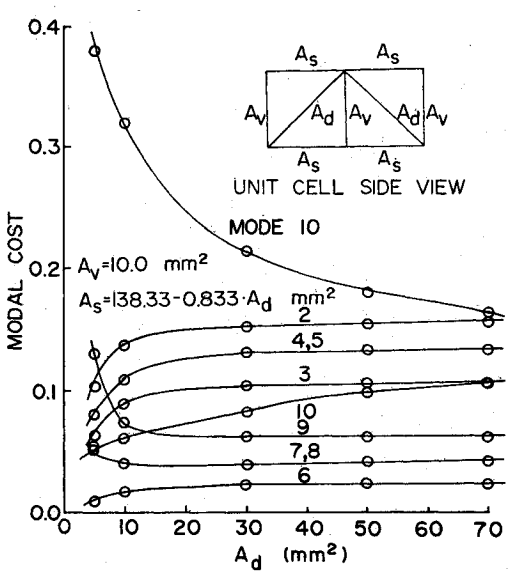

Fig. 8 Modal cost vs diagonal member area.

Thickness or Height Variation

As a second parametric study, the effect of varying the depth of the structure (h) is examined. The variation is performed such that the buckling load in the slender truss members connecting the surfaces and the total mass of the structure is held constant. For tubular members with a constant ratio of outer and inner diameters, the moment of inertia (I) is proportional to the cross-sectional area (A_v). Thus the Euler buckling load in the vertical members is held contant by maintaining a constant ratio between the cross-sectional area A_v and the height h. For simplicity, the cross-sectional area A_d is assumed to be equal to A_v.

$$A_v = A_d = (1.33 \times 10^{-6}\text{m})h \tag{26}$$

Substituting the assumed parameter values into the mass equation (22) yields the relation between A_s and h.

$$A_s = 141.2 \times 10^{-6} \frac{(h'/2) + \sqrt{1 + h'}\,)^2}{1 + (1/\sqrt{2})} \tag{27}$$

where $h' = h/7.5$ m. As h' increases, the nondimensionalized Euler buckling load in the surface members (Fig. 11) decreases, eventually indicating that these members are too slender. The natural frequencies of the first ten elastic modes of the structure are shown in Fig. 12. Note that the maximum frequency of the present ten modes occurs when h' is near 3.

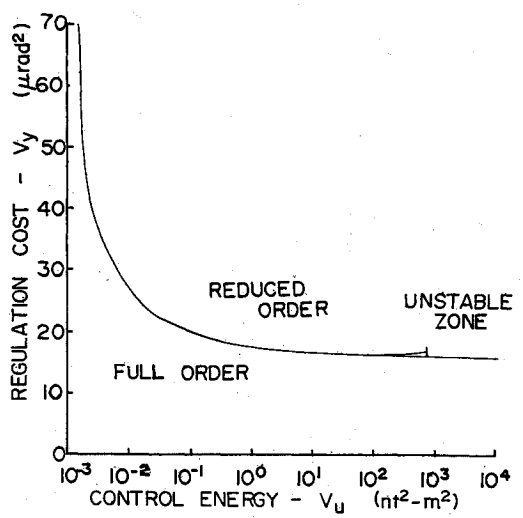

Fig. 9 Typical performance plot.

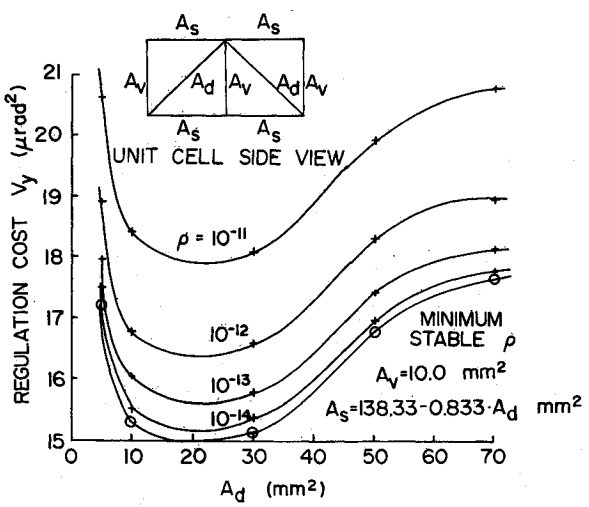

Fig. 10 System performance vs diagonal member area.

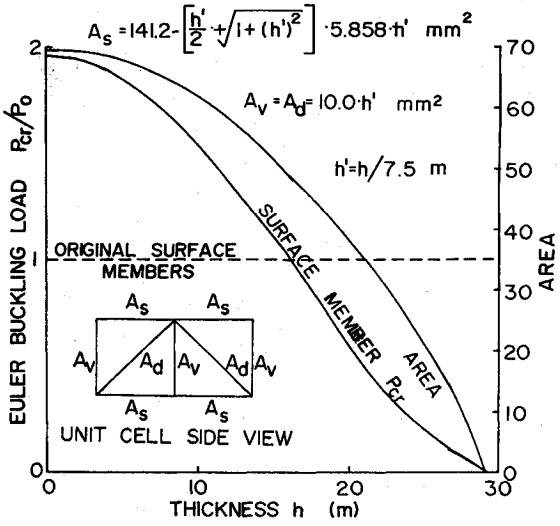

Fig. 11 Allowable buckling load vs thickness.

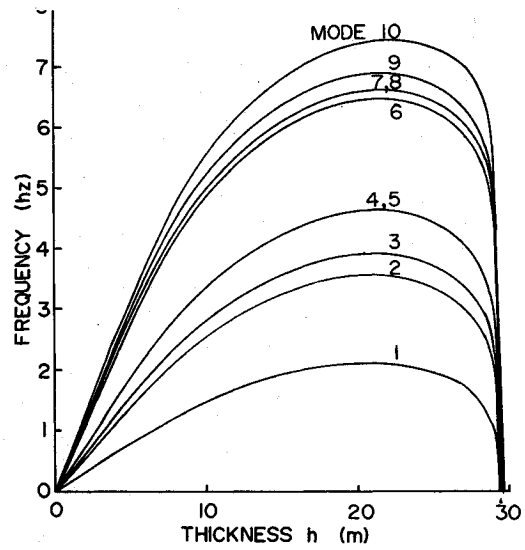

Fig. 12 Natural frequency vs thickness.

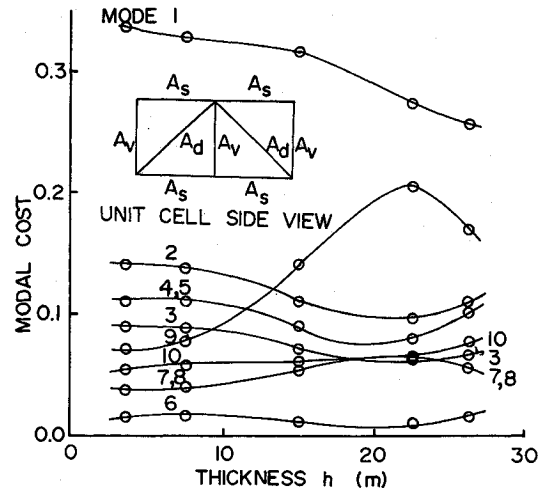

Fig. 13 Modal cost vs thickness.

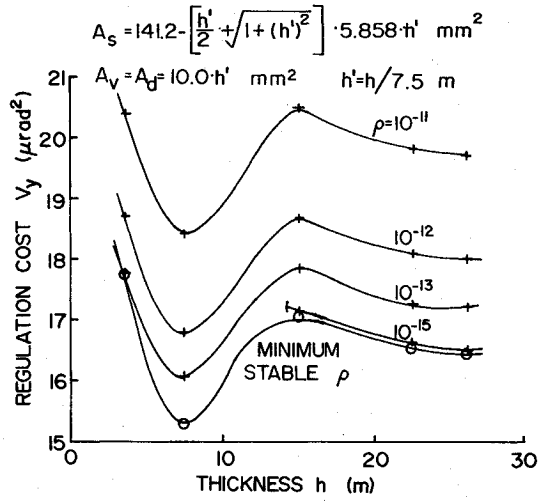

Fig. 14 System performance vs thickness.

The trend in these curves is caused by the compensating effects of A_s and h' on bending stiffness, transverse shear stiffness, and rotatory inertia. As h' increases, A_s increases [Eq. (27)]. Therefore, the increase in stiffness due to increasing h' is offset by the reduction in stiffness due to decreasing A_s.

The open-loop modal cost as a function of thickness (h) for the various modes is shown in Fig. 13. Since the modal cost curves show some crossings, different elastic modes will be retained in the reduced-order models for different ranges of thickness (h). Figure 14 shows the regulation cost (V_y) vs thickness for various constant values of ρ (+ marks) and for the minimum V_y value obtainable (circled points). The reduced-order controllers for thicknesses less that 15 m at $\rho = 1.0 \times 10^{-15}$ were unstable. The performance results are for LQG controllers based on two rigid-body modes and three elastic modes. Similar results were obtained for reduced-order controllers of other orders.[9] It is interesting to point out for this example that the optimal performance always occurs for h' near 1 with a region of worst performance for h' near 2 . The structural natural frequencies, on the other hand, are maximum for h' near 3. Again, this demonstrates the necessity of considering the closed-loop system performance when designing the structure.

Conclusion

A procedure has been demonstrated to utilize equivalent continuum finite element modeling methods to efficiently examine the effects of parametric variation of the cross sections of plate-like lattice space structures. Using a specific lattice space structural configuration, two sets of parameter variations were performed. In the first case, the length of all of the members as well as the mass of the structure were held constant. This caused the area of the surface members to be a function of the area of the thickness of the lattice space structure. Again, the length and total mass of the structure were held constant. The allowable buckling load of the slender internal members was also held constant. Thus the cross-sectional area of the surface and internal members was determined to be a function of the thickness. For both cases, maxima were obtained in the natural frequencies and optimal performance values of the design parameter were calculated. Modeling the structure using the finite element continuum model is seen to allow more flexibility in treating geometry, boundary conditions, attachments, and other structural complexities.

This procedure integrates an efficient structural dynamic analysis model into a reduced-order feedback control system design method. The present examples demonstrate the efficiency of this procedure, which may be of value to structural and control engineers. The results of the present parametric study, although incomplete, may provide some insight to both

structures and control engineers in the effect of certain geometric variations on the system performance. A logical next step is to incorporate optimization techniques into the present procedure and also to develop some representative examples.

Acknowledgments

This work was sponsored under Air Force Office of Scientific Research Contract AFOSR-83-0204, administered by Dr. Anthony Amos. The authors are deeply indebted to Professor Skelton for his help. His ideas, lectures, and discussions on modal cost analysis are the basis of this research. The authors are also indebted to Professor Corless for this help in interpreting the control system performance results.

References

[1]Sun, C. T. and Yang, T. Y., "A Continuum Approach Toward Dynamics of Gridworks," *Journal of Applied Mechanics, Transaction of ASME,* Vol. 40, No. 1, March 1973, pp. 186-192.

[2]Aswani, N., Au, N. N., and Lin, S. R., "Development of an Analytical Model for Large Space Structures," *AIAA Journal,* Vol. 20, Jan. 1982, pp. 41-48.

[3]Noor, A. K., Anderson, M. S., and Greene, W. H., "Continuum Models for Beam- and Plate-like Latticed Structures," *AIAA Journal,* Vol. 16, Dec. 1978, pp. 1219-1228.

[4]Berry, D. T., Yang, T. Y., and Skelton, R. E., "Dynamics and Control of Lattice Beams Using Simplified Finite Element Models," *Journal of Guidance, Control, and Dynamics,* Vol. 8, Sept.-Oct. 1985, pp. 612-619.

[5]Lamberson, S.E. and Yang, T.Y., "Continuum Piate Finite Elements for Vibration Analysis and Feedback Control of Large Space Structures," *Computers and Structures,* Vol. 20, No. 1-3, 1985, pp. 583-592.

[6]Bogner, F. K., Fox, R. L., and Schmit, L. A., "Generation of Interelement-Compatible Stiffness and Mass Matrices by the Use of Interpolation Formulas," *Proceedings of the First Conference on Matrix Methods in Structural Mechanics,* AFFDL TR-66-80, pp. 397-443.

[7]Skelton, R. E., "Cost Decomposition of Linear Systems with Application to Model Reduction," *International Journal of Control,* Vol. 32, No. 6, 1980, pp. 1031-1055.

[8]Kwakernaak, H. and Sivan, R., *Linear Optimal Control Systems,* 1st Ed., John Wiley & Sons, New York, 1972.

[9]Lamberson, S. E., "Continuum Plate Finite Elements for Vibration Analysis and Feedback Control of Space Lattice Structures," Ph.D. Dissertation, Purdue University, West Lafayette, IN, Aug. 1985.